EXTENDED PDF FORMAT
SPONSORED BY
Travel Grants Available
AACR Annual Meeting 2014
Application Deadline:
January 31st
>Apply Now
http://www.rndsystems.com

14-Step Synthesis of (+)-Ingenol from (+)-3-Carene

Lars Jørgensen *et al.*

Science **341**, 878 (2013);
DOI: 10.1126/science.1241606

This copy is for your personal, non-commercial use only.

If you wish to distribute this article to others, you can order high-quality copies for your colleagues, clients, or customers by clicking here.

Permission to republish or repurpose articles or portions of articles can be obtained by following the guidelines here.

The following resources related to this article are available online at www.sciencemag.org (this information is current as of February 28, 2014):

Updated information and services, including high-resolution figures, can be found in the online version of this article at:
http://www.sciencemag.org/content/341/6148/878.full.html

Supporting Online Material can be found at:
http://www.sciencemag.org/content/suppl/2013/07/31/science.1241606.DC1.html

This article **cites 34 articles**, 6 of which can be accessed free:
http://www.sciencemag.org/content/341/6148/878.full.html#ref-list-1

This article appears in the following **subject collections:**
Chemistry
http://www.sciencemag.org/cgi/collection/chemistry

Downloaded from www.sciencemag.org on February 28, 2014

Science (print ISSN 0036-8075; online ISSN 1095-9203) is published weekly, except the last week in December, by the American Association for the Advancement of Science, 1200 New York Avenue NW, Washington, DC 20005. Copyright 2013 by the American Association for the Advancement of Science; all rights reserved. The title *Science* is a registered trademark of AAAS.

depth where upward migrating Fe(II) was first detected. Given the calculated fluxes of Mn(III) and Fe(II) and the 1:1 stoichiometry in reaction 5, we estimated that up to 31% of Mn(III) can be reduced by Fe(II) at Station CE (Table 1).

$$Mn^{3+}\text{-L} + Fe^{2+} \rightarrow Mn^{2+} + Fe^{3+}\text{-L} \quad (5)$$

At stations Cabot (13%) and 16 (0.5%), this reduction pathway is less important. Although these results imply that abiotic Mn(III) reduction is important for Mn(III) removal, it is not the most important anoxic removal pathway. Nevertheless, it does have important implications for the Fe cycle, as the downward flux of Mn(III) is sufficient to oxidize the entire upward flux of Fe(II). This pathway, along with several others (*29*, *30*), also leads to soluble and/or colloidal organic Fe(III) production as shown in Fig. 1 and figs. S3 and S4 [Fe(III) = Fe_{total} – Fe(II)]. The reduction of Mn(III) by Mn-reducing bacteria, such as *S. putrefaciens* (*14*, *23*), likely accounts for the consumption of the remaining (69 to 99.5%) downward flux of Mn(III). Prior studies found a linear correlation between Mn(III) reduction and carbon oxidation (*14*, *23*), so this pathway could have implications for organic-matter mineralization. For these reasons, we have revised the current sedimentary redox paradigm (*5*) to include the above Mn(III) production and removal pathways (Fig. 2). We have also added reactions 1 and 4, as well as an unknown generalized Mn(III) microbial reduction pathway (see supplementary materials), to an established biogeochemical model of sediment diagenesis (*24*). The model results (Fig. 1, A and H) reproduce the position and shape of the soluble Mn(III) peak.

Our findings have broad implications for understanding Mn cycling in sediments. First, the current sedimentary redox model (*5*) should be revised to accommodate soluble Mn(III) and Fe(III) species. A proposed revision should highlight the importance of one-electron–transfer reactions for the Mn cycle (Fig. 2A) and explicitly consider dissolved Mn(III) and Fe(III) (Fig. 2B). Second, because Mn(III) can act as either an electron acceptor or an electron donor, the reduction-oxidation capacity of the soluble Mn pool in sediments has been underestimated. For (hemi)pelagic sediments, it appears that oxidation of Mn(II) by O_2 is an important pathway to soluble Mn(III). Soluble Mn(III) intermediates are also produced during dissimilatory MnO_2 reduction upon organic-matter mineralization and during abiotic reduction of MnO_2 by reductants such as Fe(II) and H_2S. Soluble Mn(III) is likely to be ubiquitous in sediment porewaters, where it would facilitate key electron-transfer processes in global biogeochemical cycles.

References and Notes

1. B. L. Lewis, W. M. Landing, *Deep-Sea Res.* **38**, S773–S803 (1991).
2. B. M. Tebo, *Deep-Sea Res. A, Oceanogr. Res. Pap.* **38**, S883–S905 (1991).
3. G. W. Luther III, *Geomicrobiol. J.* **22**, 195–203 (2005).
4. G. W. Luther, *Aquat. Geochem.* **16**, 395–420 (2010).
5. P. Froelich *et al.*, *Geochim. Cosmochim. Acta* **43**, 1075–1090 (1979).
6. S. Emerson *et al.*, *Geochim. Cosmochim. Acta* **46**, 1073–1079 (1982).
7. R. C. Aller, *Philos. Trans. R. Soc. Lond. A* **331**, 51–68 (1990).
8. T. J. Shaw, J. M. Gieskes, R. A. Jahnke, *Geochim. Cosmochim. Acta* **54**, 1233–1246 (1990).
9. K. S. Johnson *et al.*, *Science* **257**, 1242–1245 (1992).
10. L. N. Neretin, C. Pohl, G. Jost, T. Leipe, F. Pollehne, *Mar. Chem.* **82**, 125–143 (2003).
11. A. Schippers, L. N. Neretin, G. Lavik, T. Leipe, F. Pollehne, *Geochim. Cosmochim. Acta* **69**, 2241–2252 (2005).
12. W. B. Homoky *et al.*, *Geochim. Cosmochim. Acta* **75**, 5032–5048 (2011).
13. O. W. Duckworth, G. Sposito, *Environ. Sci. Technol.* **39**, 6037–6044 (2005).
14. J. E. Kostka, G. W. Luther, K. H. Nealson, *Geochim. Cosmochim. Acta* **59**, 885–894 (1995).
15. K. J. Klewicki, J. J. Morgan, *Environ. Sci. Technol.* **32**, 2916–2922 (1998).
16. D. L. Parker, G. Sposito, B. M. Tebo, *Geochim. Cosmochim. Acta* **68**, 4809–4820 (2004).
17. R. E. Trouwborst, B. G. Clement, B. M. Tebo, B. T. Glazer, G. W. Luther III, *Science* **313**, 1955–1957 (2006).
18. E. Yakushev, S. Pakhomova, K. Sørenson, J. Skei, *Mar. Chem.* **117**, 59–70 (2009).
19. O. Dellwig, B. Schnetger, H. J. Brumsack, H. P. Grossart, L. Umlauf, *J. Mar. Syst.* **90**, 31–41 (2012).
20. B. Schnetger, O. Dellwig, *J. Mar. Syst.* **90**, 23–30 (2012).
21. A. S. Madison, B. M. Tebo, G. W. Luther 3rd, *Talanta* **84**, 374–381 (2011).
22. P. Anschutz, B. Sundby, L. Lefrancois, G. W. Luther III, A. Mucci, *Geochim. Cosmochim. Acta* **64**, 2751–2763 (2000).
23. H. Lin, N. H. Szeinbaum, T. J. Dichristina, M. Taillefert, *Geochim. Cosmochim. Acta* **99**, 179–192 (2012).
24. B. P. Boudreau, A. Mucci, B. Sundby, G. W. Luther, N. Silverberg, *J. Mar. Res.* **56**, 1259–1284 (1998).
25. S. Mulsow, B. P. Boudreau, J. N. Smith, *Limnol. Oceanogr.* **43**, l–9 (1998).
26. S. Katsev, G. Chaillou, B. Sundby, A. Mucci, *Limnol. Oceanogr.* **52**, 2555–2568 (2007).
27. B. Sundby, N. Silverberg, R. Chesselet, *Geochim. Cosmochim. Acta* **45**, 293–307 (1981).
28. G. W. Luther III, B. Sundby, B. L. Lewis, P. J. Brendel, N. Silverberg, *Geochim. Cosmochim. Acta* **61**, 4043–4052 (1997).
29. G. W. Luther III, J. E. Kostka, T. M. Church, B. Sulzberger, W. Stumm, *Mar. Chem.* **40**, 81–103 (1992).
30. M. Taillefert, A. B. Bono, G. W. Luther, *Environ. Sci. Technol.* **34**, 2169–2177 (2000).
31. B. G. Clement, G. W. Luther III, B. M. Tebo, *Geochim. Cosmochim. Acta* **73**, 1878–1889 (2009).
32. N. P. Revsbech *et al.*, *Limnol. Oceanogr. Methods* **7**, 371–381 (2009).

Acknowledgments: This work was funded by grants from the Chemical Oceanography Division of the National Foundation to G.W.L. (OCE-1155385 and OCE-1031272) and B.M.T. (OCE-1031200 and OCE-1154307), and from the Natural Sciences and Engineering Research Council of Canada (NSERC) through Discovery and Ship-time grants to A.M. and B.S. Raw data are presented in the supplementary materials.

Supplementary Materials

www.sciencemag.org/cgi/content/full/341/6148/875/DC1
Materials and Methods
Supplementary Text
Figs. S1 to S7
Tables S1 and S2
References (*33*–*45*)

3 June 2013; accepted 29 July 2013
10.1126/science.1241396

14-Step Synthesis of (+)-Ingenol from (+)-3-Carene

Lars Jørgensen,[1]* Steven J. McKerrall,[1]* Christian A. Kuttruff,[1] Felix Ungeheuer,[1] Jakob Felding,[2] Phil S. Baran[1]†

Ingenol is a diterpenoid with unique architecture and has derivatives possessing important anticancer activity, including the recently Food and Drug Administration–approved Picato, a first-in-class drug for the treatment of the precancerous skin condition actinic keratosis. Currently, that compound is sourced inefficiently from *Euphorbia peplus*. Here, we detail an efficient, highly stereocontrolled synthesis of (+)-ingenol proceeding in only 14 steps from inexpensive (+)-3-carene and using a two-phase design. This synthesis will allow for the creation of fully synthetic analogs of bioactive ingenanes to address pharmacological limitations and provides a strategic blueprint for chemical production. These results validate two-phase terpene total synthesis as not only an academic curiosity but also a viable alternative to isolation or bioengineering for the efficient preparation of polyoxygenated terpenoids at the limits of chemical complexity.

Structurally complex, polyoxygenated terpenoids and their derivatives constitute a medicinally vital class of natural products used in a myriad of different therapeutic areas such as oncology (Taxol, Bristol-Myers Squibb), immunology (prednisone), and infectious diseases (artemisinin) (*1*). Despite the promise of complex terpenoids as drug molecules, their utility has been hampered by a number of challenges to development (*2*). In particular, many plant-derived terpenoid natural products, such as Taxol and artemisinin, suffer from a combination of low isolation yields, inconsistent isolation procedures, and nonrenewable natural sources (*3*, *4*). In the case of Taxol, plant cell culture technology overcame low-yielding isolation (*3*), whereas in the case of artemisinin, collaborations between scientists in genetic engineering and chemical synthesis hold promise for providing a consistent supply (*4*, *5*). These seminal works in the biological production of natural products have led to a widely held presumption that bioengineering

[1]Department of Chemistry, The Scripps Research Institute, 10550 North Torrey Pines Road, La Jolla, CA 92037, USA. [2]External Discovery, LEO Pharma A/S, Industriparken 55, 2750 Ballerup, Denmark.

*These authors contributed equally to this work.
†Corresponding author. E-mail: pbaran@scripps.edu

is superior to organic synthesis in the production of all complex terpenoids (*6*, *7*). Further, it has even been claimed that metabolic engineering is favored in the production of "natural products, particularly active pharmaceutical ingredients (APIs), some of which are too complex to be chemically synthesized" in a meaningful way (*7*). We repudiate these claims and present a case study in which chemical synthesis provides an approach to a structurally complex and medicinally relevant terpenoid that is both amenable to analog synthesis and concise enough to finally make chemical production possible.

A particularly chemically and biologically important terpene is ingenol (**1**, Fig. 1), a plant-derived diterpenoid first isolated by Hecker in 1968 from *Euphorbia ingens* (*8*). Its structure was elucidated through x-ray crystallography (*9*), showing a unique *in,out*-[4.4.1]bicycloundecane core, which is considerably more strained than the typical out,out configuration (*10*). In addition to its intriguing structure, ingenol esters also possess important anticancer activity in animal models and anti-HIV activity in vitro (*11*–*13*), deriving from their interaction with protein kinase C (*14*). In particular, ingenol mebutate [Picato (LEO Pharma), **2**] was recently Food and Drug Administration–approved as a first-in-class treatment for actinic keratosis (*15*), a precancerous skin condition, and has completed phase II clinical trials for the topical treatment of basal cell carcinomas (*16*). Although ingenol mebutate (**2**) is highly suited for topical applications, it is degraded through rapid ester migration and hydrolysis (*17*). These characteristics preclude systemic administration in the treatment of a broader range of cancers and are not easily addressed by available synthetic modifications of the natural product.

Currently the supply of ingenol mebutate (**2**) is limited to direct isolation (the current commercial source) and semisynthesis from ingenol (*17*, *18*). Direct isolation yields only 1.1 mg of **2** per kg of *E. peplus* (*19*), thus requiring an immense amount of plant material to achieve large-scale production. The semisynthesis requires isolation of ingenol, which, although available in a more abundant yield of 275 mg of **1** per kg of dried seeds of *E. lathyris* (*20*), still presents a dearth of material. For comparison, the isolation of artemisinin—where limited supply drives price instability—provides around 5 g per kg of dried leaves of *Artemisia annua* (*21*). In addition, engineering ingenol biosynthesis faces considerable challenges because the biosynthetic pathway is nontrivial and largely unknown [vide infra, and (*22*)]. Indeed, only the production of casbene (**4**, Fig. 2A) has been expressed in nonnative hosts, with a low titer of 31 mg/l (*23*). The above considerations led LEO Pharma, developer of Picato, to initiate a partnership with our group to design and implement a total synthesis of ingenol that would simultaneously be amenable to the creation of analogs and, more importantly, short enough to make commercial synthesis possible.

The structure and biological activity of ingenol (**1**) have motivated tremendous interest from synthetic organic chemists over the past 30 years (*24*). During that time, chemists have completed three total syntheses (*25*–*27*), one formal synthesis (*28*), and numerous approaches to the bicyclic core (*24*). Although these landmark efforts achieved elegant syntheses of **1**, those routes required between 37 and 45 steps, precluding their use in accessing synthetic analogs in meaningful quantities. As such, we required a much more concise, direct approach.

In light of the challenge of the in,out system in **1**, inspiration was sought from the biosynthesis of ingenane terpenoids (Fig. 2A). Their biosyntheses begin with the production of geranylgeranyl pyrophosphate (**3**) and its cyclization to casbene (**4**) by casbene synthase. Beyond **4**, the biosynthetic pathway remains speculative; however, the presence of a variety of intermediately cyclized natural products suggests discrete cyclizations to lathyrane, tigliane, and lastly ingenane skeletons (*22*). To the best of our knowledge, enzymes responsible for these later transformations for use in bioengineering have not been identified. The conversion from a tigliane skeleton, such as phorbol (**5,** Fig. 2B), to an ingenane skeleton should proceed through a 1,2-pinacol rearrangement, as shown with putative intermediate **6**. Cha has demonstrated this type of rearrangement by leveraging the strain of an epoxide (*29*) to overcome thermodynamic forces (vide infra). On the other hand, a vinylogous retropinacol rearrangement of ingenol (**1**) has also been observed (*30*), suggesting that the strain of the in,out system thermodynamically

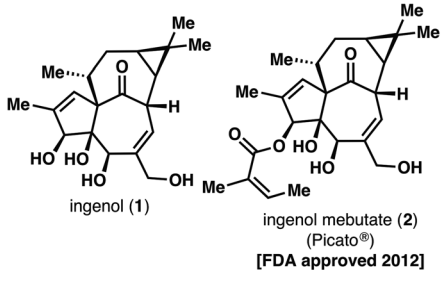

Fig. 1. Ingenol (1) and ingenol mebutate (2).

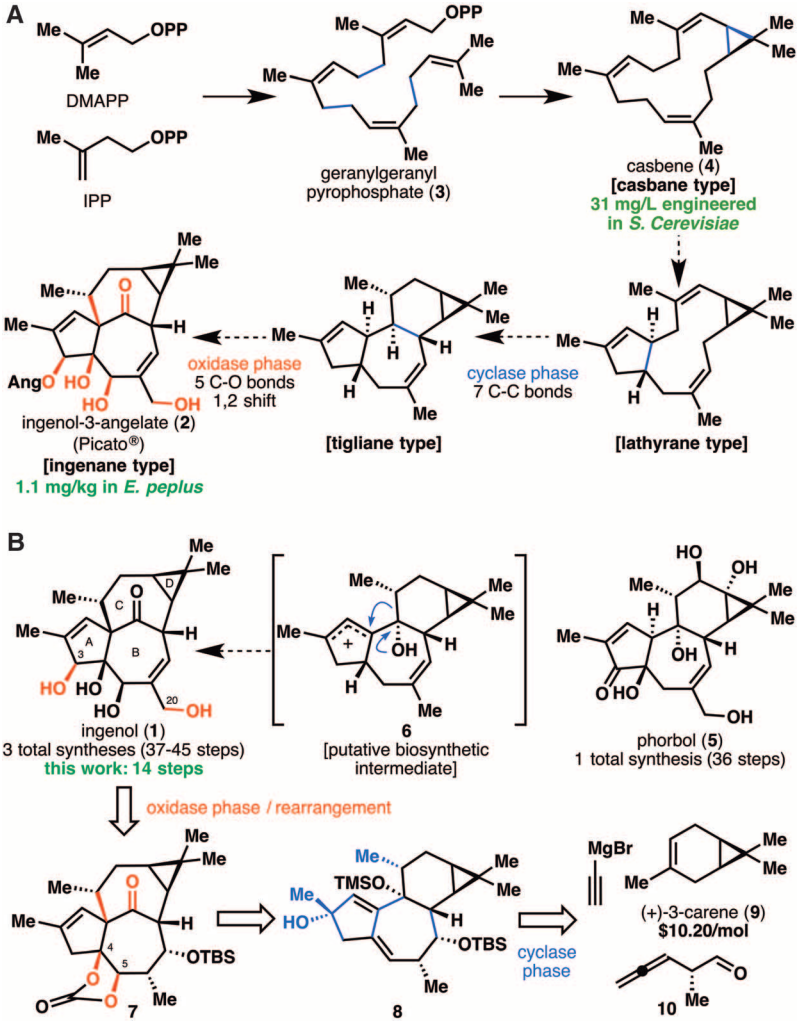

Fig. 2. Biosynthetic inspiration and retrosynthetic analysis. (**A**) Biosynthesis and bioengineering of ingenane diterpenoids. Ang is *Z*-2-methyl-2-butenoate. (**B**) Two-phase approach to ingenol.

favors the reverse reaction. Nevertheless, we viewed the vinylogous pinacol rearrangement, however challenging, as a key structurally simplifying disconnection, reducing the highly strained, bridged ring system into an angularly fused ring system.

A two-phase design consisting of a cyclase phase and an oxidase phase was chosen (*31*). The cyclase phase would establish the precursor tigliane carbon skeleton, and the oxidase phase would install the four hydroxyl groups and rearrange the tigliane skeleton to an ingenane skeleton (Fig. 2B). The retrosynthetic plan thus begins with the strategic removal of oxidized functionality in the oxidase phase. The alcohols at C-3 and C-20 were removed in anticipation that allylic oxidations would enable their installation (*32*). Indeed, Wood has demonstrated the feasibility of C-20 oxidation in his total synthesis of **1** (*27*). To conclude the oxidase phase, the remaining two alcohols (C-4 and C-5) and the in,out-bicyclic system in **7** arise from a stereoselective dihydroxylation of the corresponding olefin and a vinylogous pinacol rearrangement, respectively. In the cyclase phase, intermediate diene **8** was traced back to the commodity chemical (+)-3-carene (**9**, $10.20/mol), in which the dimethyl cyclopropane would serve as a stereochemistry-controlling element, ethynyl magnesium bromide, and aldehyde **10**. Our hypothesis was that this route would provide rapid, scalable access to diene **8**, which would serve as a key intermediate for both efficient preparation of ingenol and divergent access to ingenol analogs in sufficient quantity for drug development.

The synthesis begins with the transformation of **9** into a suitable intermediate for the installation of the C-11 methyl group and the coupling with **10** (Fig. 3). Chlorination of **9** with *N*-chlorosuccinimide (NCS), followed by ozonolysis, gave chloroketone **11** in 48% yield over two steps (22.5-g scale). The requisite methyl group could be installed through a reductive alkylation; however, the corresponding methyl ketone proved configurationally unstable and formed azeotropes with a variety of solvents, complicating its isolation. It was found that a one-pot procedure for reductive alkylation and aldol reaction provided superior isolated yield and eliminated handling of the challenging methyl ketone. Thus, **11** was treated with lithium naphthalenide followed by hexamethylphosphoramide (HMPA) and methyl

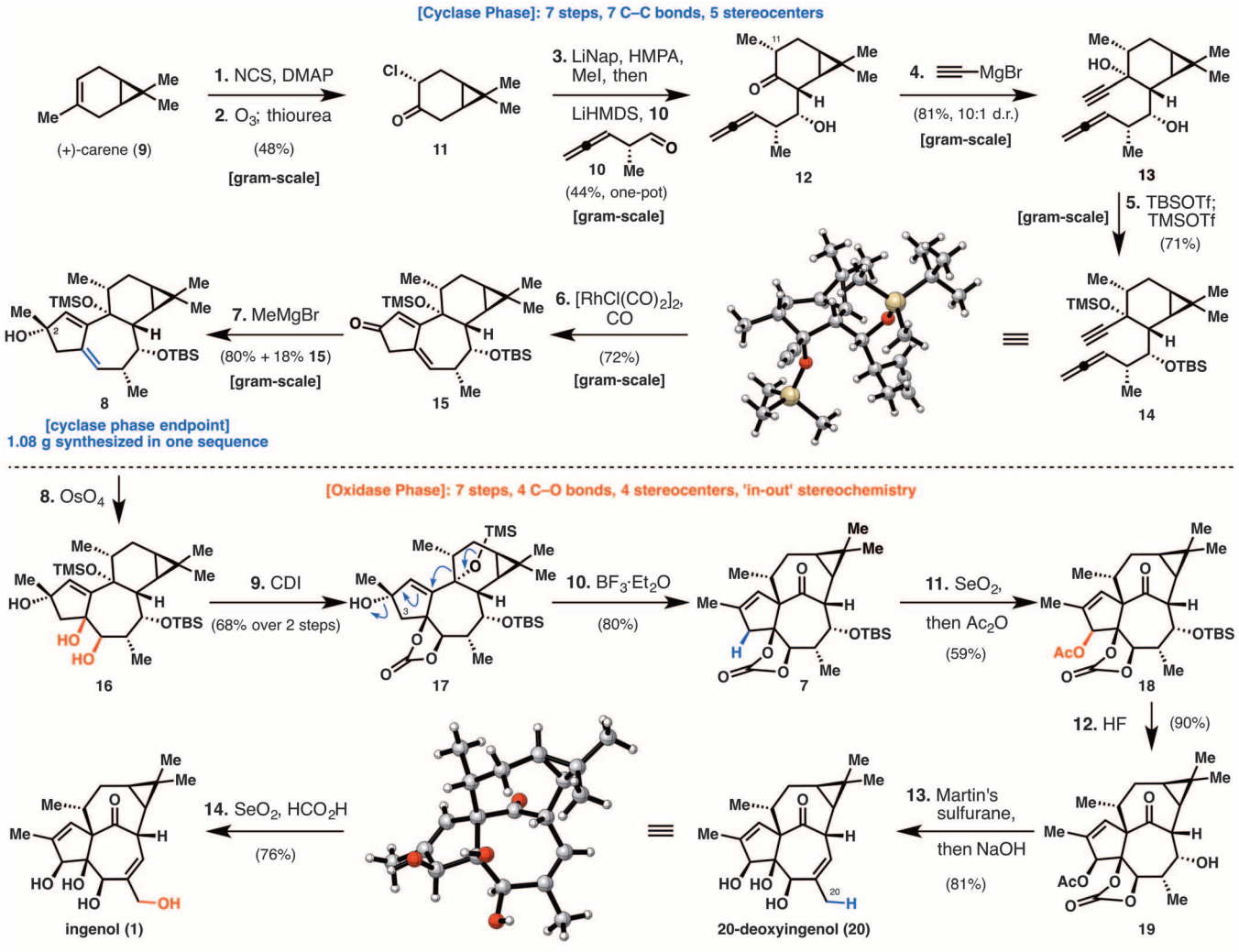

Fig. 3. Reaction sequence for the total synthesis of ingenol (1). Reagents and conditions are as follows: Reaction 1. NCS [3.0 equivalents (equiv.)], *N,N*-dimethylaminopyridine (DMAP) (0.1 equiv.), CH_2Cl_2, room temperature (r.t.), 3 hours. Reaction 2. O_3, CH_2Cl_2/MeOH; thiourea (1.6 equiv.), 2 hours, 48% over two steps. Reaction 3. Lithium naphthalenide (~2 equiv.), MeI (10 equiv.), HMPA/tetrahydrofuran (THF), –78°C to r.t., 1.5 hours; LiHMDS (1.25 equiv.), **10** (2.0 equiv.), –78°C, 4 hours, 44%. Reaction 4. Ethynylmagnesium bromide (5.0 equiv.), THF, –78° to –15°C, 3 hours, 81%. Reaction 5. TBSOTf (2.0 equiv.), Et_3N (4.0 equiv.), CH_2Cl_2, 0°C, 30 min; TMSOTf (2.0 equiv.), Et_3N (4.0 equiv.), 0°C, 1.5 hours, 71%. Reaction 6. $[RhCl(CO)_2]_2$ (0.1 equiv.), *p*-xylene, 140°C, 12 hours, 72%. Reaction 7. Methylmagnesium bromide (4.1 equiv.), THF, –78° to 0°C, 30 min, 80% + 18% **15**. Reaction 8. OsO_4 (1.5 equiv.), pyridine, r.t., 12 hours; 1:1 aqueous Na_2SO_3/THF, r.t., 12 hours. Reaction 9. CDI (5.0 equiv.), DMAP (0.1 equiv.), CH_2Cl_2, r.t., 8 hours, 64% over 2 steps. Reaction 10. BF_3•Et_2O (10.0 equiv.), CH_2Cl_2, –78° to –40°C, 30 min, then Et_3N/MeOH, 80%. Reaction 11. SeO_2 (5.0 equiv.), dioxane, 80°C, 14 hours; Ac_2O (20.0 equiv.), DMAP (0.1 equiv.), pyridine (40.0 equiv.), r.t., 1 hour, 59%. Reaction 12. HF (60.0 equiv.), CH_3CN, 50°C, 10 hours, 90%. Reaction 13. Martin's sulfurane (6.0 equiv.), $CHCl_3$, 80°C, 3 hours, then NaOH, THF, 1 hour, 81%. Reaction 14. SeO_2 (10.0 equiv.), 2:1 dioxane/formic acid, 80°C, 1.25 hours, then NaOH, 76%.

iodide. The excess methyl iodide was removed by distillation, and subsequent addition of lithium bis (trimethylsilyl)amide (LiHMDS) and **10**—derived from 2-iodoxybenzoic acid (IBX) oxidation of the corresponding alcohol (*33*)—delivered aldol product **12** as a single diastereomer in 44% yield (6.4-g scale).

Treatment of **12** with ethynyl magnesium bromide provided diol **13** in 81% yield as a 10:1 mixture of diastereomers (3.0-g scale). This initial four-step sequence rapidly assembles **13**, the substrate for the key Pauson-Khand cyclization, by setting four contiguous stereocenters and forming three carbon–carbon bonds. Under known conditions (*34*) for the Pauson-Khand cyclization, **13** decomposed rapidly. The alcohols were identified as problematic functionalities and were protected by sequential, one-pot treatment with *tert*-butyldimethylsilyl triflate (TBSOTf) and trimethylsilyl triflate (TMSOTf) to deliver **14** in 72% yield (2.7-g scale). Unexpectedly, **14** crystallized upon cooling, and x-ray crystallographic analysis unambiguously confirmed the desired stereochemistry. Aided by the pioneering studies of Brummond and others on allenic Pauson-Khand reactions (*34*), cyclization of **14** was effected by treatment with 10 mole percent (mol %) $[RhCl(CO)_2]_2$ under a CO atmosphere to provide dienone **15** in 72% yield (1.5-g scale). The use of degassed and anhydrous solvent under high dilution (0.005 M) conditions proved essential to the high yield of this reaction.

Installation of the C-2 methyl group was achieved by treatment of **15** with methylmagnesium bromide to give **8**, the cyclase phase end point, in 80% yield with an additional 18% recovered **15** (1.3-g scale). By using the described route, 1.08 g of **8** was prepared in a single sequence. The cyclase phase proceeded in only seven steps from **9** to generate five stereocenters and form seven carbon–carbon bonds, illustrating the strategic value of targeting a minimally oxidized core structure and using powerful carbon–carbon bond–forming methodologies.

The oxidase phase began with the dihydroxylation of **8**. Unfortunately, catalytic dihydroxylation was ineffective on **8**, and only starting material or overoxidation product was obtained under numerous conditions used. Dihydroxylation of the desired olefin could be realized through the use of stoichiometric OsO_4, followed by reductive hydrolysis, to deliver the requisite diol **16** as a single stereoisomer. The crude diol **16** was protected with *N*,*N*-carbonyldiimidazole (CDI) to deliver carbonate **17** in 68% yield over two steps (100-mg scale). With **17** in hand, conditions were developed for the pivotal vinylogous pinacol rearrangement. Initial results were disappointing because **17** was unreactive or underwent elimination under conditions used. However, it was discovered that reaction temperature plays a crucial role. The desired pinacol rearrangement could ultimately be effected by treating **17** with BF_3•Et_2O (where Et indicates an ethyl group) in CH_2Cl_2 at –78° to –40°C, followed by quenching with Et_3N and MeOH (Me, methyl), to set the strained in,out stereochemistry and produce ingenane **7** in 80% yield (191-mg scale). These results, in light of previous reports of the retropinacol rearrangement (*30*) of ingenol (**1**), suggest competing kinetic and thermodynamic factors. Efforts to understand the dynamics of this reaction and its implications for ingenol (**1**) biosynthesis are ongoing.

The C-3 alcohol was installed by allylic oxidation with SeO_2, followed by in situ protection as the acetate, to deliver **18** as a single diastereomer in 59% yield (128-mg scale). Removal of the TBS group with HF gave alcohol **19** in 90% yield (82-mg scale). An x-ray crystal structure, obtained by conversion of **19** to the *para*-bromobenzoate **21**, unambiguously confirmed the stereochemistry of both the alcohol triad and the *in,out* bicyclic system (Fig. 4A). Alcohol elimination and global deprotection were achieved by treatment with Martin's sulfurane, followed by basic hydrolysis, to provide crystalline 20-deoxyingenol (**20**) in 80% yield (23-mg scale). Installation of the final C-20 alcohol was accomplished by using Shibuya's conditions for allylic oxidation (*35*)—which produced higher conversion, without overoxidation, than Wood's conditions (*27*)—to deliver **1** in 76% yield (10-mg scale). Synthetic **1** and **20** were spectroscopically identical to naturally obtained material. Thus, the oxidase phase consists of seven steps, which install the congested tetraol moiety and use a biomimetic rearrangement to generate the all-carbon quaternary stereocenter and in,out stereochemistry. The use of late-stage oxidations to introduce the four alcohols, particularly those that involve functionalization of activated C–H bonds, greatly increases the step economy of the synthesis (*36*).

A synthesis of **1** was achieved in 14 steps and 1.2% overall yield (73% average per step) from **9**. This compares favorably with the 1.1 mg/kg [0.0011% weight/weight (w/w)] isolation yield of **2** (*18*) and the 275 mg/kg (0.028% w/w) isolation yield of **1** (*19*). Salient features of the current route include (i) a four-step sequence transforming **9** into stereochemically complex **13**, (ii) a catalytic allenic Pauson-Khand reaction producing the core carbon skeleton, (iii) a seemingly improbable (*30*) vinylogous pinacol rearrangement setting the requisite in,out stereochemistry, and (iv) sequential, chemoselective oxidation reactions installing the alcohol tetrad. A notable feature of the synthesis is excellent redox economy, evidenced by the absence of nonstrategic redox manipulations (*37*). Additionally, the approach provides gram quantities of key intermediate **8**, which serves as a point of divergence for the synthesis of analogs of **2** (vide infra). Such studies are ongoing, and the current synthesis is being scaled up in conjunction with LEO Pharma to produce large quantities of intermediate **8** for use in analog preparation.

This synthesis of **1** is not without limitations. In particular, the oxidase phase relies on the use of stoichiometric quantities of toxic oxidants (OsO_4 and SeO_2) to install the alcohol functionality. A first step to address these issues is a catalytic dihydroxylation of dienone **15** (Fig. 4B), which uses 5 mol % OsO_4 in the presence of citric acid, to deliver diol **22** in 88% yield (180-mg scale). The use of these conditions on the dihydroxylation of **8** gave decomposition, however, and retailoring the synthesis to use **22** requires a change in protecting group strategy. These challenges point to limitations in existing chemical methods for oxidation (*31*), and additional efforts to address the scalability of the oxidase phase are ongoing.

The oxidase phase shown is designed to yield **1**; however, by using the predictable oxidase reactivity exemplified above, intermediate **8** can be diverted to a variety of ingenanes of varying oxidation and substitution patterns to address the pharmacological challenges to oral dosing of **2**. By altering the oxidase phase, we can

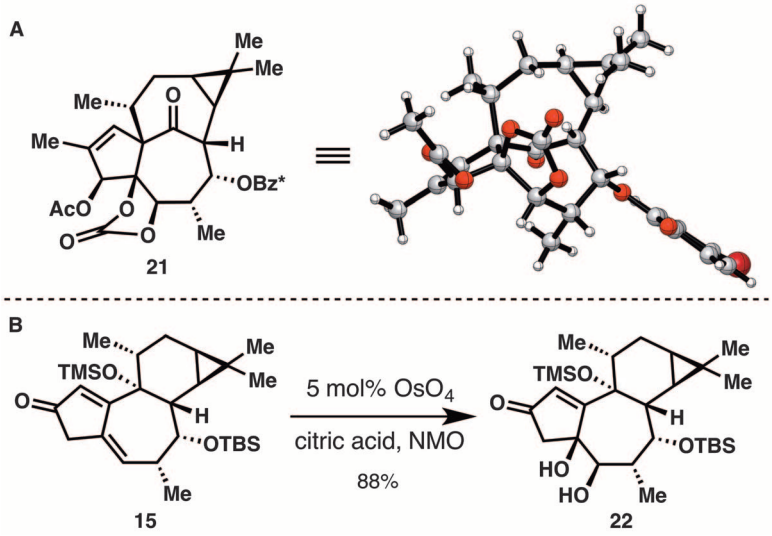

Fig. 4. Stereochemical confirmation and preliminary catalytic dihydroxylation. (**A**) X-ray crystal structure of **21**. Bz* is *p*-bromobenzoate. (**B**) Catalytic dihydroxylation of **15**. OsO_4 (0.05 equiv.), *N*-methylmorpholine *N*-oxide (NMO) (2.0 equiv.), citric acid (2.0 equiv.), 1:1 *t*-BuOH/H_2O, r.t., 24 hours, 88%.

produce analogs of **2** differing in the alcohol functionalities (C-3, C-4, C-5, and C-20) to better understand the structure-activity relationship of ingenanes.

The synthesis of ingenol (**1**) presented herein illustrates the power of two-phase logic to deliver an efficient, concise synthesis even in architecturally complex settings. The usefulness of the two-phase approach will undoubtedly continue to expand as new methods for C–C bond formation and C–H oxidation are developed. Furthermore, this report provides a strong rebuttal to the presumption that chemical synthesis is ill-equipped to deal with the preparation of structurally complex terpenoid drug molecules. Rather, in this instance, total chemical synthesis holds promise as the best method to both prepare ingenol mebutate (**2**) and enable the development of therapeutic analogs with broader utility in the treatment of human diseases.

References and Notes

1. F. E. Koehn, G. T. Carter, *Nat. Rev. Drug Discov.* **4**, 206–220 (2005).
2. I. Raskin *et al*., *Trends Biotechnol.* **20**, 522–531 (2002).
3. P. G. Mountford, in *Green Chemistry in the Pharmaceutical Industry*, P. J. Dunn, A. S. Wells, M. T. Williams, Eds. (Wiley, Weinheim, Germany, 2010), pp. 145–160.
4. C. J. Paddon *et al*., *Nature* **496**, 528–532 (2013).
5. C. Zhu, S. P. Cook, *J. Am. Chem. Soc.* **134**, 13577–13579 (2012).
6. J. D. Keasling, A. Mendoza, P. S. Baran, *Nature* **492**, 188–189 (2012).
7. J. D. Keasling, *Science* **330**, 1355–1358 (2010).
8. E. Hecker, *Cancer Res.* **28**, 2338–2349 (1968).
9. K. Zechmeister *et al*., *Tetrahedron Lett.* **11**, 4075–4078 (1970).
10. R. W. Alder, S. P. East, *Chem. Rev.* **96**, 2097–2112 (1996).
11. S. M. Ogbourne *et al*., *Cancer Res.* **64**, 2833–2839 (2004).
12. M. Fujiwara *et al*., *Antimicrob. Agents Chemother.* **40**, 271–273 (1996).
13. A. Vasas, D. Rédei, D. Csupor, J. Molnár, J. Hohmann, *Eur. J. Org. Chem.* **2012**, 5115–5130 (2012).
14. C. M. Hasler, G. Acs, P. M. Blumberg, *Cancer Res.* **52**, 202–208 (1992).
15. U.S. Food and Drug Administration, *2012 Novel New Drugs Summary* (FDA, Washington, DC, 2013); www.fda.gov/downloads/Drugs/DevelopmentApprovalProcess/DrugInnovation/UCM337830.pdf.
16. G. Siller *et al*., *Australas. J. Dermatol.* **51**, 99–105 (2010).
17. "European public assessment report: Picato" [European Medicines Agency (EMA) publication 650464, London, 2012]; www.ema.europa.eu/docs/en_GB/document_library/EPAR_-_Public_assessment_report/human/002275/WC500135329.pdf.
18. X. Liang, G. Grue-Sørensen, A. K. Petersen, T. Högberg, *Synlett* **23**, 2647–2652 (2012).
19. J. Hohmann, F. Evanics, L. Berta, T. Bartók, *Planta Med.* **66**, 291–294 (2000).
20. G. Appendino, G. C. Tron, G. Cravotto, G. Palmisano, J. Jakupovic, *J. Nat. Prod.* **62**, 76–79 (1999).
21. V. Hale, J. D. Keasling, N. Renninger, T. T. Diagana, *Am. J. Trop. Med. Hyg.* **77** (suppl.), 198–202 (2007).
22. R. J. Schmidt, *J. Linn. Soc. Bot.* **94**, 221–230 (1987).
23. J. Kirby *et al*., *Phytochemistry* **71**, 1466–1473 (2010).
24. I. Kuwajima, K. Tanino, *Chem. Rev.* **105**, 4661–4670 (2005).
25. J. D. Winkler, M. B. Rouse, M. F. Greaney, S. J. Harrison, Y. T. Jeon, *J. Am. Chem. Soc.* **124**, 9726–9728 (2002).
26. K. Tanino *et al*., *J. Am. Chem. Soc.* **125**, 1498–1500 (2003).
27. A. Nickel *et al*., *J. Am. Chem. Soc.* **126**, 16300–16301 (2004).
28. K. Watanabe *et al*., *J. Org. Chem.* **69**, 7802–7808 (2004).
29. O. L. Epstein, J. K. Cha, *Angew. Chem. Int. Ed.* **44**, 121–123 (2004).
30. G. Appendino *et al*., *Eur. J. Org. Chem.* **1999**, 3413–3420 (1999).
31. K. Chen, P. S. Baran, *Nature* **459**, 824–828 (2009).
32. A. Nakamura, M. Nakada, *Synthesis* **45**, 1421–1451 (2013).
33. T. Konegawa, Y. Ohtsuka, H. Ikeda, T. Sugai, H. Ohta, *Synlett* **1997**, 1297–1299 (1997).
34. K. M. Brummond *et al*., *Org. Lett.* **4**, 1931–1934 (2002).
35. K. Shibuya, *Synth. Commun.* **24**, 2923–2941 (1994).
36. P. A. Wender, V. A. Verma, T. J. Paxton, T. H. Pillow, *Acc. Chem. Res.* **41**, 40–49 (2008).
37. N. Z. Burns, P. S. Baran, R. W. Hoffmann, *Angew. Chem. Int. Ed.* **48**, 2854–2867 (2009).

Acknowledgments: Financial support for this work was provided by LEO Pharma. The Carlsberg Foundation and the Danish Council for Independent Research (Technology and Production Sciences) provided postdoctoral fellowships for L.J., and the Alexander von Humboldt Foundation provided a postdoctoral fellowship for C.A.K. We are grateful to A. Rheingold and C. E. Moore (University of California, San Diego) for x-ray crystallographic analysis and G. Siuzdak (the Scripps Research Institute) for mass spectrometry assistance. We thank H. Bladh (LEO Pharma) for valuable discussions and LEO Pharma for generous donations of natural 20-deoxyingenol and ingenol. Metrical parameters for the structures of compounds **14**, **20**, and **21** are available free of charge from the Cambridge Crystallographic Data Centre under reference numbers CCDC-943074, 943076, and 943075, respectively. A provisional patent application has been filed and is available under patent application no. U.S. 61/829,861.

Supplementary Materials

www.sciencemag.org/cgi/content/full/science.1241606/DC1
Materials and Methods
Supplementary Text
Figs. S1 to S4
Tables S1 to S7
Data

7 June 2013; accepted 18 July 2013
Published online 1 August 2013;
10.1126/science.1241606

Mapping of Functional Groups in Metal-Organic Frameworks

Xueqian Kong,[1,2]* Hexiang Deng,[3,4]*† Fangyong Yan,[1,4]* Jihan Kim,[4]‡ Joseph A. Swisher,[1,4] Berend Smit,[1,3,4] Omar M. Yaghi,[3,4,5]§ Jeffrey A. Reimer[1,2]§

We determined the heterogeneous mesoscale spatial apportionment of functional groups in a series of multivariate metal-organic frameworks (MTV-MOF-5) containing BDC (1,4-benzenedicarboxylate) linkers with different functional groups—B (BDC-NH_2), E (BDC-NO_2), F [(BDC-$(CH_3)_2$], H [BDC-$(OC_3H_5)_2$], and I [BDC-$(OC_7H_7)_2$]—using solid-state nuclear magnetic resonance measurements combined with molecular simulations. Our analysis reveals that these methods discern between random (EF), alternating (EI and EHI), and various cluster (BF) forms of functional group apportionments. This combined synthetic, characterization, and computational approach predicts the adsorptive properties of crystalline MTV-MOF systems. This methodology, developed in the context of ordered frameworks, is a first step in resolving the more general problem of spatial disorder in other ordered materials, including mesoporous materials, functionalized polymers, and defect distributions within crystalline solids.

A strategy for optimizing the properties of synthetic crystalline materials is to deliberately introduce heterogeneity by increasing the number of constituents (*1*). This approach can be compromised by the dual challenges of phase separation, lack of order, or both. Multivariate metal-organic frameworks (MTV-MOFs) can meet this challenge by incorporating multiple linkers that bear different functional groups into the same crystal, which creates a heterogeneous interior (*2*). This heterogeneity can enhanced selectivity for carbon dioxide (CO_2) capture and hydrogen uptake relative to mixtures of pure materials. On a fundamental level, these materials present characterization challenges, in that there are no experimental techniques that can elucidate the intermingling of functional groups that characterizes the heterogeneity within the crystalline MTV-MOFs. For example, this "heterogeneity problem" is intractable for diffraction methods (x-ray, neutron, and electron) and remains unexamined with other characterization methods. We show that multidimensional solid-state nuclear magnetic resonance (SSNMR) combined with molecular simulations can be used to generate three-dimensional (3D) maps of the apportionment of functional groups (Fig. 1) within and between the pores of MTV-MOF-5. These MTV-MOFs adopt MOF-5 structure containing BDC (1,4 benzenedicarboxylate) linkers with different functional groups–B (BDC-NH2), E (BDC-NO2), F [(BDC-(CH3)2], H [BDC-(OC3H5)2], and I [BDC-(OC7H7)2]. This method can be applied to other ordered or disordered systems to

[1]Department of Chemical and Biomolecular Engineering, University of California, Berkeley, CA 94720, USA. [2]Environmental Energy Technologies Division, Lawrence Berkeley National Laboratory, Berkeley, CA 94720, USA. [3]Department of Chemistry, University of California, Berkeley, CA 94720, USA. [4]Materials Sciences Division, Lawrence Berkeley National Laboratory, Berkeley, CA 94720, USA. [5]NanoCentury KAIST Institute and Graduate School of Energy, Environment, Water, and Sustainability (World Class University), Daejeon 305-701, Republic of Korea.

*These authors contributed equally to this work.
†Present address: College of Chemistry and Molecular Sciences, Wuhan University Luojiashan, Wuhan, 430072 China.
‡Present address: Department of Chemical and Biomolecular Engineering, Korea Advanced Institute of Science and Technology, 291 Daehak-ro Yuseong-gu, Daejeon, 305-701 Korea.
§Corresponding author. E-mail: yaghi@berkeley.edu (O.M.Y.); reimer@berkeley.edu (J.A.R.)